Available online at www.sciencedirect.com
SCIENCE DIRECT®
Journal of Solid State Chemistry 177 (2004) 1276–1284
JOURNAL OF SOLID STATE CHEMISTRY
http://elsevier.com/locate/jssc

High-pressure single-crystal X-ray diffraction study of $YAlO_3$ perovskite

N.L. Ross,* J. Zhao, and R.J. Angel

Crystallography Laboratory, Department of Geosciences, Virginia Polytechnic Institute and State University, Blacksburg, VA 24061, USA

Received 7 September 2003; accepted 5 November 2003

Abstract

The equation of state and structural changes of $YAlO_3$ perovskite, a $GdFeO_3$-type perovskite with *Pbnm* symmetry, have been investigated to 8.5 GPa in a diamond-anvil cell at room temperature using single-crystal X-ray diffraction. A fit of a third-order Birch-Murnaghan equation of state to the $P-V$ data yields values of $K_{T0} = 192(2)$ GPa and $K'_0 = 7.3(4)$, with compressional moduli of the axes, $K_{a0} = 220(7)$ GPa, $K_{b0} = 157(3)$ GPa and $K_{c0} = 212(2)$ GPa, and their pressure derivatives, $K'_{a0} = 12(2)$, $K'_{b0} = 4.4(6)(6)$ and $K'_{c0} = 8.7(4)$. The evolution of the structure with pressure shows that compression of the YO12 site is strongly anisotropic with the four longest Y–O separations more compressible than the eight shorter Y–O bond lengths. Consequently the distortion of the YO12 site decreases with increasing pressure. In contrast, the AlO6 site undergoes nearly isotropic compression and is more compressible than the YO12 site. The interoctahedral angles, ∠ Al–O1–Al and ∠ Al–O2–Al, show a significant increase with pressure, reflected in the movement of O1 along ⟨100⟩. The structure of $YAlO_3$ perovskite therefore becomes less distorted with increasing pressure, in contrast with other *Pbnm* perovskites such as $CaSnO_3$.

Keywords: $YAlO_3$ perovskite; High pressure; Crystal structure; Equation of state; Single crystal; X-ray diffraction

1. Introduction

The orthorhombic $GdFeO_3$-type perovskites (*Pbnm*), with general stoichiometry ABO_3, are derived from the ideal cubic structure (*Pm*3*m*) via the titling and distortion of the *B*O6 octahedra (e.g., [1–3]). The perovskites are of great interest in materials science because the relatively simple crystal structure displays many diverse electric, magnetic, piezoelectric, optical, catalytic, and magnetoresistive properties. Doped $YAlO_3$ perovskite crystals, for example, serve as very efficient laser hosts. In addition, perovskites are of interest in earth science because $(Mg,Fe)SiO_3$ transforms to a perovskite structure with *Pbnm* symmetry at high pressures and temperatures and is believed to form the bulk of the Earth's lower mantle (e.g., [4]). Studies of $GdFeO_3$-type perovskites at high pressure provide a useful probe of the atomistic controls on structural changes in this important class of materials.

A previous study of $YAlO_3$ perovskite to ~4 GPa suggested that the AlO6 octahedra are more compressible than the YO12 site and that the Al–O–Al octahedral tilting decreases with pressure [5]. However, the structural changes reported were just at the limits of the experimental resolution and contrasted with other studies of $GdFeO_3$-type perovskites that showed increases in distortion with increasing pressure [6,7]. Recently several improvements have been made to reduce the uncertainties in structural parameters determined from X-ray diffraction measurements of single crystals loaded in a diamond anvil cell to the level approaching that obtained from crystals in air. Thus insights into the evolution of the structure in relatively stiff materials like $YAlO_3$ at high pressure can now be achieved [8]. We have therefore re-investigated the high-pressure behavior of $YAlO_3$ to 8.5 GPa and determined both the equation of state and evolution of the structure with pressure. In particular, we address the questions of how the tilting and distortion of the AlO6 octahedra changes with pressure, the atomistic factors that control relative compressibility of the YO12 and AlO6 sites, and how these affect the overall changes in the distortion of the structure.

*Corresponding author. Fax: +1-540-231-3386.
E-mail address: nross@vt.edu (N.L. Ross).

0022-4596/$ - see front matter © 2003 Elsevier Inc. All rights reserved.
doi:10.1016/j.jssc.2003.11.014

2. Experimental methods

A synthetic $YAlO_3$ sample was kindly supplied by Division of Mineralogy, Smithsonian Museum. Single crystals for the equation of state study and structural study were selected after X-ray diffraction measurements in air that confirmed that no twinning was present. Experimental details of the equation of state measurements and high-pressure structure determinations are given below.

2.1. Equation of state

The high-pressure equation of state measurements were performed with a BGI-design diamond-anvil cell [9]. A 200 μm-thick T301 steel gasket was preindented to a thickness of 90 μm and a hole of $\phi = 350$ μm was drilled in the center of the indented region. A crystal with dimensions of $80 \times 90 \times 40$ μm was loaded into the diamond-anvil cell together with a ruby chip for approximate pressure measurements and a quartz crystal with dimensions of $100 \times 90 \times 40$ μm that served as an internal diffraction pressure standard. A 4:1 mixture of methanol:ethanol was used as the pressure medium. The constant widths of the diffraction peaks at all pressures indicated that this pressure medium remained hydrostatic up to the highest pressures achieved, ~8 GPa. Diffraction measurements were performed on a Huber four-circle diffractometer as described in Ref. [10]. Unit-cell parameters were determined at each pressure from a least-squares fit to the corrected setting angles of 18–20 reflections obtained by the eight-position centering method [11]. The unconstrained unit-cell angles showed no significant deviation from 90°, indicating that the structure remains orthorhombic over the pressure range of our data. The values of symmetry-constrained unit-cell parameters obtained by vector-least-squares [12] are reported in Table 1. Pressures were determined from the unit-cell volumes of the quartz crystal in the diamond anvil cell, using the Birch-Murnaghan third-order equation of state with $K_{T0} = 37.12(9)$ GPa, and $K_0' = 5.99(4)$ reported by Angel et al. [13]. Equation of state parameters were obtained by a weighted-least-squares fit of the Birch-Murnaghan third-order equation of state to the pressure-volume data [14]. Weights for each datum were calculated by the effective variance method [15] from the *esd* in the unit-cell volume of the perovskites combined with the uncertainty in pressure corresponding to the *esd* of the unit-cell volume of the quartz pressure standard.

2.2. Structure evolution at high pressure

A second diamond anvil cell without a quartz crystal was used for the high-pressure structure measurements, enabling a larger $YAlO_3$ crystal to be loaded. A $YAlO_3$ plate with dimensions of 155×130 μm was oriented parallel to (110) and polished to ~32 μm thickness in order to gain access to the maximum number of reflections along the crystallographic axes. The crystal was loaded with (110) parallel to the surface of a 600 μm anvil of an ETH diamond anvil cell [16] and a 4:1 methanol:ethanol mixture served as the pressure-transmitting medium. A 200 μm-thick T301 steel gasket was preindented to a thickness of 110 μm and a hole of $\phi = 328$ μm was drilled in the center of the indented region. A ruby sphere was loaded into the cavity to serve as a pressure calibrant [17]. Uncertainties in pressure were estimated from the difference between measurements before and after data collections. Unit cell parameters were also measured on a Huber four-circle diffractometer using the 8-position-centering technique described above. The pressures calculated from the equation of state are in good agreement with those measured with the ruby fluoresence method.

Intensity data for all accessible reflections were collected at room pressure (in the DAC) and at 1.05, 2.59, 3.791, 5.089, 6.31, 7.11 and 7.94 GPa using ω scans with the fixed-ϕ mode [18] from 2° to 40° in θ on an Xcalibur diffractometer (Mo$K\alpha$, 50 kV, 40 mA). We determined the offset of the crystal from the rotation axis of the goniometer by measuring between 20 and 40 strong low-angle reflections and calculating the crystal offsets from the reflection positions with the WinIntegrStp program [19]. We found that it was critical to eliminate these offsets by adjusting the DAC on the goniometer before data collection in order to obtain accurate reflection intensities. Peak fitting and integration of intensities were carried out by using the WinIntegrStp software. Corrections to the intensities for the absorption effects of the DAC, including correction of beryllium plates, diamond anvils, shadowing by the gasket and the sample itself, were made by using ABSORB 5.3 (www.crystal.vt.edu/crystal/software) which is based on Burnham's [20] methods and original code. After the crystallographically equivalent reflections were averaged, the remaining independent reflections with ($F > 4\sigma(F)$) were used to refine structures with

Table 1
Unit cell parameters of $YAlO_3$ perovskite at high pressure

P (GPa)	a (Å)	b (Å)	c (Å)	V (Å^3)
0.0001	5.17868(29)	5.32953(49)	7.37002(21)	203.412(16)
1.556(4)	5.16785(27)	5.31190(63)	7.35237(27)	201.830(21)
1.850(4)	5.16473(20)	5.30859(38)	7.34937(15)	201.501(12)
2.739(5)	5.15906(17)	5.29899(30)	7.33983(12)	200.655(9)
3.605(6)	5.15293(24)	5.29083(42)	7.33134(17)	199.876(13)
4.706(7)	5.14594(16)	5.27918(28)	7.32027(11)	198.865(9)
6.133(6)	5.13684(15)	5.26567(26)	7.30660(10)	197.636(8)
7.575(5)	5.12895(22)	5.25195(39)	7.29401(15)	196.479(12)
8.814(9)	5.12181(14)	5.24045(24)	7.28285(10)	195.476(7)

Table 2
Refinement information for $YAlO_3$ perovskite at high pressures

P (GPa)	0.0	1.05(2)	2.59(2)	3.791(4)	5.09(1)	6.31(3)	7.11 (6)	7.94 (8)
$N(>2I_0/\sigma(I_0))$[a]	666	663	698	666	662	600	571	604
$N(F>4\sigma(F))$[b]	230	235	205	196	198	182	176	190
$R_{int}(N)$[c]	0.0168	0.0206	0.0185	0.0227	0.0193	0.0231	0.0184	0.019
	(203)	(205)	(191)	(185)	(184)	(168)	(150)	(175)
G_{fit}[d]	0.90	1.08	1.06	1.15	1.01	0.88	0.88	1.01
Extinction factor ($\times 10^{-4}$)	0.17(1)	0.16(1)	0.16(1)	0.13(1)	0.14(1)	0.20(1)	0.16(2)	0.17(1)
R_w[e]	0.019	0.025	0.021	0.026	0.020	0.020	0.018	0.021
R_{uw}[f]	0.018	0.022	0.020	0.033	0.019	0.022	0.019	0.020

[a] Number of reflections with $I>2I_0/\sigma(I_0)$.
[b] R_{int}, Number of independent reflections with $F>4\sigma(F)$.
[c] Internal residual on F (Number of averaged reflections).
[d] Estimated standard deviation of unit weight observation.
[e] Weighted $R_w = [\sum w(|F_o| - |F_c|)^2/\sum|F_o|^2]^{1/2}$.
[f] Unweighted $R_{uw} = \sum||F_o| - |F_c||/\sum|F_o|$.

RFINE99, a development version RFINE4 [21]. Details of all refinement information, the refined positions of atoms and thermal parameters and distances and angles are listed in Tables 2–4.

3. Results

3.1. Equation of state

The volume of $YAlO_3$ perovskite decreases smoothly with increasing pressure, with no evidence of any phase transitions throughout the pressure range studied (Fig. 1a). The fit of the $P-V$ data collected between room pressure and 8.814(9) GPa yielded room pressure parameters $V_0 = 203.403(17)$ Å^3, $K_{T0} = 192.1(1.8)$ GPa and $K_0' = 7.3(4)$ for the third-order Birch-Murnaghan equation of state with a weighted $\chi^2 = 1.63$. Fig. 1b shows the compression data plotted as normalized pressure, F, against the Eulerian strain measure, f [14]. $F-f$ plots provide a visual indication of whether higher order terms such as K_0' and K_0'' are significant in the EoS. If all data points lie on a horizontal line of constant F, for example, then $K_0' = 4$, and the data can be fitted with a second-order Birch-Murnaghan EoS. If the data lie on an inclined straight line, as is the case for $YAlO_3$, the data will be adequately described by a third-order truncation of the Birch-Murnaghan EoS with the slope of each line equal to $3K_T(K'-4)/2$. Fig. 1b therefore provides visual confirmation that K_0' is significantly greater than 4 for $YAlO_3$, similar to other orthorhombic perovskites [22–24]. Fitting the data for any of these materials with a second-order EoS (i.e., $K_0' = 4$) leads to significantly worse fits to the data and significant over-estimates of the bulk moduli.

The elastic moduli of the individual unit-cell axes of $YAlO_3$ perovskite were also obtained from the measured data by fitting a third-order Birch-Murnaghan equation of state to the cubes of each of the cell parameters [14]. The resulting axial moduli (K_{d0}) and their pressure derivatives (K_{d0}') are $K_{a0} = 219(7)$ GPa, $K_{b0} = 157(3)$ GPa and $K_{c0} = 212(2)$ GPa, with $K_{a0}' = 11.5(1.7)$, $K_{b0}' = 4.4(6)$ and $K_{c0}' = 8.7(5)$. Thus the b-axis is significantly more compressible than either c or a.

3.2. Structural evolution with pressure

Fig. 2 displays the variation of the Al–O bond lengths, $R_{ij}(P)$, with increasing pressure. Slopes of the bond lengths (dR_{ij}/dP) were obtained from a linear least-squares fitting and the linear compressibilities at room pressure that were calculated using the relationship, $-1/R_{ij}(0)\ dR_{ij}/dP$. The Al–O1 and Al–O22 bond lengths have similar compressibilities within resolution of measurement, whereas the longer Al–O21 bond is slightly more compressible (Table 5). As a consequence, the degree of distortion within the AlO6 octahedra shows a slight decrease with pressure, as indicated by the quadratic elongation (λ) and bond-angle variance (σ) parameters that are equal to 1 and 0, respectively for a regular octahedron [25]. At room pressure, the AlO6 octahedra in $YAlO_3$ are close to being regular with $\lambda = 1.0002$ and $\sigma = 0.63$. At 7.94 GPa, the AlO6 are slightly less distorted, with $\lambda = 1.0001$ and $\sigma = 0.25$. The observation that the octahedral distortion decreases with increasing pressure is consistent with the earlier study [5].

The compression of the YO12 dodecahedral site is more anisotropic than the AlO6 octahedron (Table 5). The four longer Y–O distances are more compressible than the eight shorter Y–O bond distances and thus the distortion of YO12 decreases with increasing pressure. The observed bond length distortion $\Delta_i(=1/n \times \Sigma\{(R_{ij} - \langle R_i \rangle)/\langle R_i \rangle\}^2 \times 10^3$, where $\langle R_i \rangle$ is the average bond length, R_{ij} is an individual bond length

Table 3
Unit cell parameters, refined positional parameters and anisotropic temperature factors (β_{ij}) and equivalent isotopic temperatures factors (B_{eq}) of $YAlO_3$ perovskite at high pressure

P (GPa)	0.0	1.05(2)	2.59(2)	3.791(4)	5.09(1)	6.31(3)	7.11 (6)	7.94 (8)
a (Å)	5.18027(38)	5.17197(38)	5.16098(34)	5.15299(34)	5.14492(42)	5.13657(34)	5.13188(33)	5.12731(37)
b (Å)	5.32951(16)	5.31791(20)	5.30102(18)	5.28875(18)	5.27614(20)	5.26397(15)	5.25676(15)	5.24899(17)
c (Å)	7.37059(12)	7.35884(15)	7.34181(16)	7.32979(16)	7.31715(18)	7.30511(13)	7.29840(14)	7.29083(15)
V (Å^3)	203.489(12)	202.398(12)	200.861(10)	199.758(10)	198.627(12)	197.521(10)	196.889(10)	196.220(11)
Y[a]								
x	−0.01192(7)	−0.01191(8)	−0.01158(9)	−0.01164(8)	−0.01134(8)	−0.01107(7)	−0.01105(8)	−0.01108(9)
y	0.05305(7)	0.05256(9)	0.05195(10)	0.05149(11)	0.05093(9)	0.05040(9)	0.05019 (8)	0.04989(9)
B_{eq}	0.420(11)	0.428(15)	0.398(14)	0.405(8)	0.389(14)	0.437(15)	0.419(14)	0.404(15)
$\beta 11$	0.00422(31)	0.0057(4)	0.0040(3)	0.0051(4)	0.0041(4)	0.0038(4)	0.0052(4)	0.0050(5)
$\beta 22$	0.00345(22)	0.0027(3)	0.0029(3)	0.0023(4)	0.00272(29)	0.0034(3)	0.0028(2)	0.0028(3)
$\beta 33$	0.00191(5)	0.00171(7)	0.00204(8)	0.00186(6)	0.0020(7)	0.00250(8)	0.00192(7)	0.00181(7)
$\beta 12$	−0.00037(7)	−0.00033(8)	−0.00027(10)	−0.00041(13)	−0.00041(10)	−0.00027(9)	−0.0003(10)	−0.00019(10)
Al[b]								
B_{eq}	0.342(20)	0.390(26)	0.336(24)	0.326(24)	0.320(25)	0.322(25)	0.304(19)	0.284(27)
$\beta 11$	0.0013(10)	0.0049(12)	0.0029(9)	0.0028(12)	0.0017(11)	0.0004(11)	0.0010 (5)	0.0011(12)
$\beta 22$	0.0047(7)	0.0024(8)	0.0029(8)	0.0020(10)	0.0034(7)	0.0045(7)	0.0032(5)	0.0033(8)
$\beta 33$	0.00159(13)	0.00170(19)	0.00170(19)	0.00207(24)	0.00186(18)	0.00198(19)	0.00203(19)	0.00187(20)
$\beta 12$	−0.00001(18)	0.00005(21)	−0.00021(26)	0.0001(3)	−0.00003(23)	−0.00041(23)	−0.00001(22)	0.00053(23)
$\beta 13$	0.00013(19)	0.00030(26)	0.00024(23)	−0.0005(3)	−0.00038(27)	−0.00002(24)	−0.00019(23)	−0.00017(26)
$\beta 23$	0.00004(18)	0.00028(27)	0.00013(29)	0.0004(3)	−0.00017(25)	0.00001(3)	0.00020(23)	0.00016(26)
O1[c]								
x	0.0840(6)	0.0828(8)	0.8322(8)	0.0824(10)	0.0822(8)	0.0836(8)	0.0811(8)	0.0817(8)
y	0.4775(5)	0.4801(6)	0.4805(8)	0.4805(7)	0.4805(7)	0.4805(6)	0.4797(6)	0.4812(7)
B_{eq}	0.51(4)	0.53(4)	0.35(5)	0.41(6)	0.43(5)	0.51(5)	0.45(5)	0.50(6)
$\beta 11$	0.0056(17)	0.0080(22)	0.0034(23)	0.0078(28)	0.0016(23)	0.0045(19)	0.0037(20)	0.0039(24)
$\beta 22$	0.0040(12)	0.0034(13)	0.0024(21)	0.0008(29)	0.0072(21)	0.0056(15)	0.0070(20)	0.0075(21)
$\beta 33$	0.0021(3)	0.0017(4)	0.0019(3)	0.0014(5)	0.0015(4)	0.0020(4)	0.0010(4)	0.0012(4)
$\beta 12$	0.0003(6)	−0.0001(7)	0.0003(7)	0.0009(9)	−0.0009(7)	−0.0008(8)	0.0002(7)	0.0002(8)
O2								
x	0.7049(3)	0.7048(5)	0.7054(4)	0.7050(6)	0.7057(5)	0.7058(4)	0.7054(4)	0.7053(5)
y	0.2949(3)	0.2944(4)	0.2933(5)	0.2935(6)	0.2947(4)	0.2934(4)	0.2939(4)	0.2941(4)
z	0.0441(2)	0.0438(3)	0.0431(3)	0.0429(4)	0.0427(3)	0.0428(3)	0.0424(3)	0.0426(3)
B_{eq}	0.47(3)	0.46(4)	0.46(5)	0.48(4)	0.44(4)	0.50(4)	0.45(4)	0.42(4)
$\beta 11$	0.0044(11)	0.0058(16)	0.0049(15)	0.0077(20)	0.0031(18)	0.0073(16)	0.0050(15)	0.0048(18)
$\beta 22$	0.0043(7)	0.0027(10)	0.0028(14)	0.0009(20)	0.0040(14)	0.0012(13)	0.0025(13)	0.0028(14)
$\beta 33$	0.0021(2)	0.0021(3)	0.0024(3)	0.0024(4)	0.00250(26)	0.0027(2)	0.0025(3)	0.0021(3)
$\beta 12$	−0.0007(4)	−0.0010(5)	−0.0003(6)	−0.0008(6)	−0.0000(5)	−0.0003(5)	0.0005(3)	−0.0009(6)
$\beta 13$	0.0010(3)	0.0004(4)	−0.0001(4)	−0.0002(4)	−0.0001(4)	0.0009(4)	0.0002(4)	0.0001(4)
$\beta 23$	−0.0005(3)	−0.0004(3)	0.0006(5)	0.0005(5)	−0.0004(4)	−0.0004(4)	0.0001(4)	0.0005(5)

[a] Y: $z = 0.25; \beta 13 = \beta 23 = 0$.
[b] Al: $x = 0.0$, $y = 0.5$, $z = 0.5$.
[c] O1: $z = 0.25; \beta 13 = \beta 23 = 0$.

and n is the number of the bond [26]), decreases from 20.17 to 18.57 between room pressure and 8 GPa.

In order to compare the relative compression of the two sites, the polyhedral bulk moduli, K_P of AlO6 and YO12 were obtained by fitting the polyhedral volumes with the Birch-Murnaghan finite-strain formulism [14] using the EOSFit program (www.crystal.vt.edu/crystal/software). The resulting $V_{0,poly}$, K_{P0} and K'_P are 9.273(16) Å^3, 177(6) GPa and 4.1(1.2) for AlO6 and 41.589(19) Å^3, 208(5) GPa and 4.1 (1.4) for YO12. The volume compressibility of the YO12 site ($\beta_{YO12} = 1/K_P$), $\beta_{YO12} = 4.81(12) \times 10^{-3}$ GPa^{-1}, is therefore ~15% less than that of the AlO6 octahedron ($\beta_{AlO6} = 5.65(19) \times 10^{-3}$ GPa^{-1}).

The interoctahedral Al–O1–Al (α_1) and Al–O2–Al (α_2) angles both increase with increasing pressure (Fig. 3a). Other angle parameters have been introduced to describe the tilting [27–29] such as the tilt of the octahedra about the pseduo-cubic $\langle 110 \rangle$ p-axis, θ, and the tilt of the of the octahedra about the pseduo-cubic

Table 4
Interatomic distances (Å), angles(°), and polyhedral volumes of AlO6, V_{oct} (Å^3), and YO12, V_{dod} (Å^3), of $YAlO_3$ perovskite at high pressure

P (GPa)	0.00	1.052(24)	2.591(21)	3.791(4)	5.089(13)	6.31(3)	7.11 (6)	7.94 (8)
Al–O1 × 2	1.8972(07)	1.8920(9)	1.8884(9)	1.8838(12)	1.8804(9)	1.8789(9)	1.8748(9)	1.8728(10)
Al–O22 × 2	1.9074(16)	1.905 (2)	1.901 (2)	1.898 (3)	1.888 (2)	1.888 (2)	1.8850(20)	1.8836(21)
Al –O21 × 2	1.9240(16)	1.917 (2)	1.908 (2)	1.904 (3)	1.8804(9)	1.898 (2)	1.8950(20)	1.8941(20)
V_{oct}	9.280(21)	9.213(26)	9.131(29)	9.075(33)	9.024(25)	8.974(25)	8.928(23)	8.908(24)
O1–Al–2 × 2	88.97(10)	89.15(12)	89.17(13)	89.31(16)	89.30(13)	89.46(12)	89.15(13)	89.34(14)
O1–Al–O2 × 2	89.19(9)	89.58(12)	89.23(13)	89.48(16)	89.43(13)	89.33(13)	89.40(12)	89.57(13)
O1–Al–O1 × 2	180.00	180.00	180.00	180.00	180.00	180.00	180.00	180.00
O1–Al–O2 × 2	90.81(9)	90.42(12)	90.77(13)	90.52(16)	90.57(13)	90.67(13)	90.60(12)	90.43(13)
O1–Al–O2 × 2	91.03(10)	90.85(12)	90.83(13)	90.69(16)	90.70(13)	90.54(12)	90.85(13)	90.66(14)
O2–Al–O2 × 2	90.16(2)	90.14(3)	90.14(3)	90.15(4)	90.25(3)	90.25(3)	90.24(03)	90.30(3)
O2–Al–O2 × 2	89.84(2)	89.86(3)	89.86(3)	89.85(4)	89.75(3)	89.75(3)	89.76(03)	89.70(3)
O2–Al–O2 × 2	180.00	180.00	180.00	180.00	180.00	180.00(0)	180.00	180.00
Y–O1 I	2.316(3)	2.326(3)	2.315(3)	2.320(4)	2.317(3)	2.316(3)	2.306(3)	2.313(4)
Y–O1 ii	2.253(3)	2.252(4)	2.245(4)	2.243(5)	2.239(4)	2.226(4)	2.237(4)	2.231(4)
Y–O1 iii	2.991(3)	2.978(4)	2.976(4)	2.965(5)	2.960(4)	2.964(4)	2.947(4)	2.948(4)
Y–O1 iv	3.108(3)	3.083(3)	3.078(3)	3.058(5)	3.048(3)	3.039(3)	3.035(3)	3.023(4)
Y–O2 v × 2	2.279(18)	2.277(2)	2.277(2)	2.271(3)	2.264(2)	2.263(2)	2.260(2)	2.254(2)
Y–O2 vi × 2	2.473(17)	2.471(2)	2.465(2)	2.465(3)	2.464(2)	2.458(2)	2.460(2)	2.458(2)
Y–O2 vii × 2	2.572(16)	2.567(2)	2.561(2)	2.555(3)	2.549(2)	2.548(2)	2.542(2)	2.540(2)
Y–O2 viii × 2	3.2662(19)	3.2562)	3.237(3)	3.2303()	3.223(2)	3.211(2)	3.207(2)	3.205(2)
V_{dod}	41.592(18)	41.386(23)	41.084(27)	40.865(37)	40.633(22)	40.406(23)	40.294(21)	40.147(21)
Al–O1–Al	152.46(18)	153.03(24)	152.80(23)	153.18 (30)	153.22(24)	152.81(24)	152.81(24)	153.54(22)
Al–O2–Al	151.82(10)	152.00(14)	152.42(15)	152.41(19)	152.37(13)	152.81(24)	152.56(13)	152.54(13)

$\langle 001 \rangle$ p-axis, ϕ (Fig. 3b), that are equivalent to the rotation angle, Φ, introduced by O'Keeffe et al. [27]. From Fig. 3b, we see that ϕ decreases slightly within the resolution of the measurement, whereas θ shows a more obvious decrease with pressure. Therefore tilting of the AlO6 in $YAlO_3$ perovskite at high pressure is mainly controlled by rotation of θ which results in displacement of O1 atoms along $\langle 100 \rangle$ (Fig. 4). All tilt parameters therefore indicate that the structure is becoming less distorted with increasing pressure.

4. Discussion

The unit cell compression of an orthorhombic perovskite such as $YAlO_3$ and the relative compressibility of both the octahedral (AlO6) and dodecahedral (YO12) sites are intimately related. From a geometric point of view, the length of one of the three pairs of Al–O bonds can be expressed as

$$R_{Al-O1} = \frac{c}{4\sin(\alpha_1/2)}. \quad (1)$$

If an average bond length, R_{Al-O2}, is substituted for R_{Al-O21} and R_{Al-O22}, we can also obtain:

$$R_{Al-O2} = \frac{\sqrt{a^2+b^2}}{4\sin(\alpha_2/2)}. \quad (2)$$

These relationships lead directly to the following expressions for bond compressibilities:

$$\beta_{Al-O1} = \beta_c + \frac{1}{\sin(\alpha_1/2)}\left(\frac{d\sin(\alpha_1/2)}{dP}\right), \quad (3)$$

$$\beta_{Al-O2} = \beta_{ab} + \frac{1}{\sin(\alpha_2/2)}\left(\frac{d\sin(\alpha_2/2)}{dP}\right), \quad (4)$$

where

$$\beta_{ab} = \frac{(a^2+kb^2)\beta_a}{(a^2+b^2)}$$

and $k = \beta_b/\beta_a$. From (3) and (4), it is clear that compression of R_{Al-O1} is controlled by compression of c and α_1 whereas compression of R_{Al-O2} is controlled by compression of a, b and α_2.

Because the compressibility of the dodecahedral site is essentially represented by the compression of the unit-cell, one can now use these equations to explore the inter-relationship of the octahedral tilts represented by the α angles and the relative compressibilities of the octahedral and dodecahedral sites. For example, one extreme of possible behavior is represented by the "rigid-unit" model, in which the octahedra undergo no internal distortion or compression and the compressibilities of the Al–O bonds are zero. In this case Eqs. (3) and (4) indicate that the values of α_1 and α_2 must decrease with increasing pressure, meaning that the

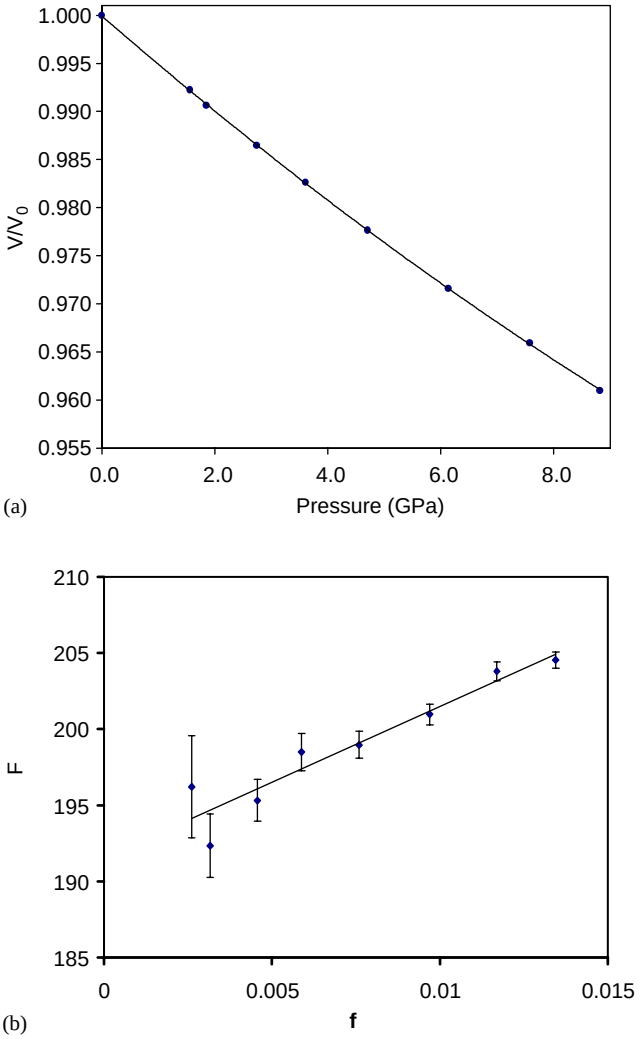

Fig. 1. (a) Variation of the volume of $YAlO_3$ perovskite with pressure at room temperature and (b) normalized stress–strain ($F-f$) plots derived from the measured volumes for a Birch-Murnaghan EoS.

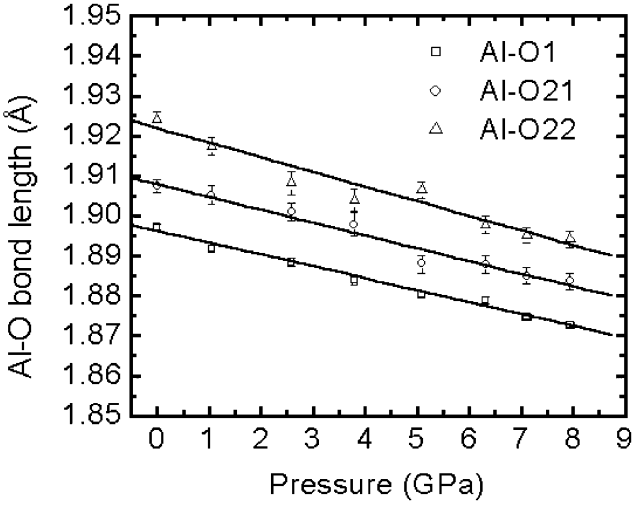

Fig. 2. The variation of the Al–O bond distances as a function of pressure.

octahedra become *more tilted* with increasing pressure. As shown in Fig. 3a, our experimental data show that this is clearly not the case for $YAlO_3$, and confirms that the decrease in octahedral tilting that we find is related to the compression of the Al–O bonds. Decreased octahedral tilting means that $d \sin \alpha_i / dP > 0$. Eqs. (3) and (4) indicate that for this to occur the octahedra must be more compressible than the unit-cell parameters. Essentially this means that for the tilts to decrease with increasing pressure, the octahedra must be more compressible than the dodecahedral site.

Further understanding of the components of the mechanisms of the structural compression of orthorhombic perovskites can be obtained by examining one further model, which we previously introduced in our analysis of the high-pressure behavior of $CaSnO_3$ perovskite [8]. This model is built on the assumption that a, b, and c of the perovskite unit cell vary as the measured variations with increasing pressure, but the fractional coordinates (x, y, z) of the atoms within the asymmetric unit do not change with pressure. This "fixed coordinate" model provides insight into how the real structure changes under pressure by showing how a "driving force" optimizes the geometric configuration of structure of model by shifting atomic coordinates or moving atoms to the equilibrium positions found in the real structure. As we will see, this is clearly equivalent to tilting of the octahedral AlO6 and distortions in YO12 and AlO6 sites.

For $YAlO_3$ the "fixed coordinate" model predicts that two of the three Al–O bonds are less compressible than the measured values (Table 5, Fig. 5). For example, the mean linear compressibility of Al–O from the model, $\beta^m_{\mathrm{Al-O}} = 1.44(2) \times 10^{-3}\,\mathrm{GPa}^{-1}$, is less than the observed value, $\beta_{\mathrm{Al-O}} = 1.72(10) \times 10^{-3}\,\mathrm{GPa}^{-1}$. For the YO12 site, the model predicts that the average compressibility of the eight shortest Y–O bonds, $1.52(5) \times 10^{-3}\,\mathrm{GPa}^{-1}$, is similar to the average compressibility of the four longer Y–O distances, $1.56(2) \times 10^{-3}\,\mathrm{GPa}$, compared with the observed values of $1.11(9) \times 10^{-3}\,\mathrm{GPa}$ and $2.45(15) \times 10^{-3}\,\mathrm{GPa}$, respectively. This difference must therefore be ascribed to a shift of the Y atom along $\langle 010 \rangle$ and the octahedral tilts which are not taken into account in the model. Thus the "fixed coordinate" model predicts an almost isotropic compression for YO12 with YO12 more compressible than AlO6 whereas the observed compression of YO12 is anisotropic with AlO6 more compressible than YO12.

As a consequence of the anisotropic compression of YO12, the bond angles Al–O1–Al (α_1) and Al–O2–Al (α_2) are observed to increase with pressure. The Y–O bonds with the highest compressibilities [Y–O13 (iii), Y–O14 (iv), Y–O23 (vii) and Y–O24 (viii)] and those with the lowest compressibilities [Y–O11(i), Y–O13(iii),Y–O21(v) and Y–O22(vi)] are directly related to the octahedral tilting (Table 4). The "fixed

Table 5
Slopes of variation of Al–O and Y–O distances with pressure for the observed structure and "fixed atom" reference model

Interatomic distance		R_i (Å) at room pressure	$\Delta R_{ij}/\Delta P$ (Å/GPa) experiment	$\Delta R_{ij}/\Delta P$ (Å/GPa) model	Observed linear compressibility β ($\times 10^{-3}$ GPa^{-1})	Model linear compressibility β ($\times 10^{-3}$ GPa^{-1})
Al–O1 ($\times 2$)		1.8972(7)	−0.00297(12)	−0.00255(5)	1.57(6)	1.34(2)
Al–O21 ($\times 2$)		1.9240(17)	−0.0037(3)	−0.00329(5)	1.92(15)	1.71(2)
Al–O22 ($\times 2$)		1.9074(17)	−0.0032(2)	−0.00287(5)	1.68(10)	1.50(2)
Average		1.910(8)			1.72(10)	1.44(2)
Y–O11	i	2.316(2)	−0.0010(6)	−0.00436(6)	0.4(3)	1.88(2)
Y–O12	ii	2.253(3)	−0.0030(5)	−0.00298(6)	1.3(2)	1.32(2)
Y–O13	iii	2.991(3)	−0.0052(6)	−0.00394(8)	1.7(2)	1.32(2)
Y–O14	iv	3.108(3)	−0.0101(7)	−0.00590(9)	3.2(2)	1.90(2)
Y–O21 ($\times 2$)	v	2.2792(18)	−0.0030(5)	−0.00351(5)	1.3(2)	1.54(2)
Y–O22 ($\times 2$)	vi	2.4731(17)	−0.0018(2)	−0.00368(5)	0.73(8)	1.49(2)
Y–O23 ($\times 2$)	vii	2.5723(16)	−0.0041(2)	−0.00359(6)	1.59(8)	1.40(2)
Y–O24 ($\times 2$)	viii	3.2662(19)	−0.0080(3)	−0.00492(8)	2.45(9)	1.51(2)
$\langle AO \rangle$	vii	2.402			1.11(9)	1.51(6)
$\langle AO \rangle$	xii	2.654			1.57(2)	1.52(5)

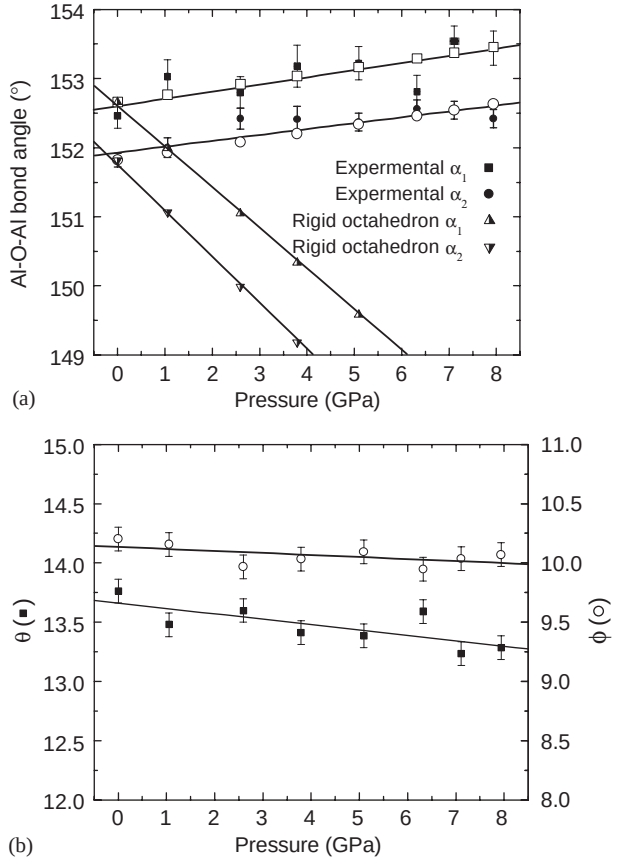

Fig. 3. (a) Pressure evolution of the octahedral tilt angles, Al–O1–Al and Al–O2–Al, of $YAlO_3$ perovskite at high pressure (solid symbols), where the hollow symbols represent angles calculated using: $\alpha_i = 2\sin^{-1}(\exp(\Delta\beta_i P)\sin\alpha_{0i}/2)$ and assuming rigid AlO6 octahedra; (b) Pressure dependence of titling angles, θ and φ (see text for details).

coordinate" model, however, predicts that α_1 and α_2 do not change significantly with increasing pressure. From room pressure to 7.94 GPa, α_1 and α_2 are calculated to vary from 152.47° to 152.48° and 151.82° to 151.79°, respectively. Thus no significant octahedral tilting is predicted by the fixed-coordinate model. It is clear that if one only considers the axial compression of the unit cell without adjustment of atomic positional coordinates, an incorrect model is obtained for the observed structural variation of $YAlO_3$ perovskite. The shifts of atomic positions are required in order to ensure that AlO6 becomes more compressible than YO12 which is equivalent to an increase in tilting between AlO6 (α_1 and α_2) and a decrease in distortion of both AlO6 and the YO12.

Because there is no obvious variation of α_1 and α_2 with pressure in the "fixed coordinate" structure, the Al–O bond compressibilities of the model are only determined by β_a, β_b, and β_c. For AlO6 to be more compressible than the YO12, it is necessary for β_b to be greater than β_a (see Eq. (4)), which is consistent with experimental results. So, in this sense, the relative compressibilities of the unit-cell axes a and b can be predicted by knowing the relative compressibilities of the octahedral and dodecahedral sites, provided the change in tilt angles is small. However, as shown above, the relative compression of AlO6 and YO12 cannot solely be considered from unit cell compression without adjustment of atomic positions.

Finally it is worth pointing out that the evolution of Al–O1–Al and Al–O2–Al with pressure can be obtained by calculating the difference of $\Delta\beta_1(=\beta_{\mathrm{Al-O1}}-\beta_c)$ and $\Delta\beta_2(=\beta_{\mathrm{Al-O2}}-\beta_{ab})$ and using $\alpha_i = 2\sin^{-1}(\exp(\Delta\beta_i P)\sin\alpha_{0i}/2)$, where α_{0i} is the value of α_i at room pressure. The angles calculated could be more precise than those obtained from the structure refinement because $\Delta\beta_i$ might reduce possible systematic errors in measured $\beta_{\mathrm{Al-Oi}}$ and $\beta_{a,b,c}$. Fig. 3a displays the observed and calculated angles as a function of pressure where

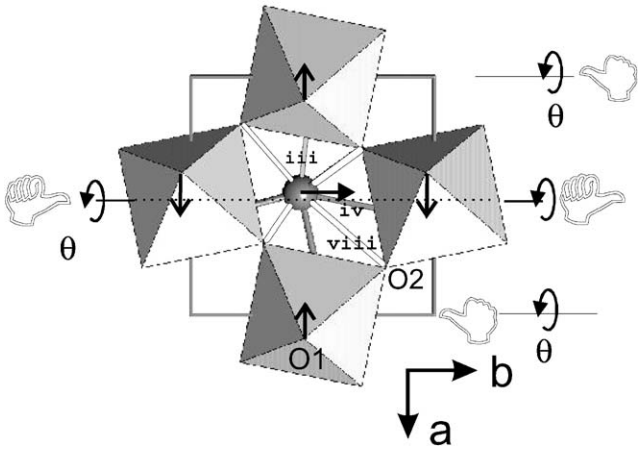

Fig. 4. Structure of $YAlO_3$ perovskite showing the effect of pressure, including tilting of the AlO6 octahedra and displacement of O1 and Y atoms. Y–O2 bonds are shown in gray and Y–O1 bonds are shown white. The four longer Y–O distances (Y–O1 iii, Y–O1 iv and Y–O2 viii) are also labeled.

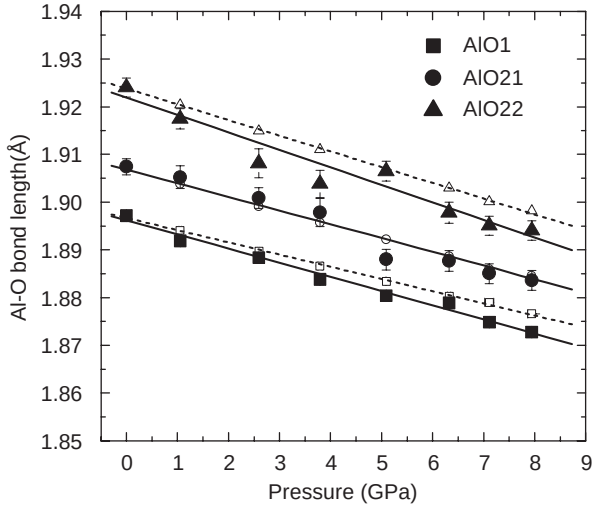

Fig. 5. Comparison of compressibility of the Al–O bonds between the observed structure (solid symbols) and the "fixed atom" reference structure (hollow symbols).

$\Delta\beta_1 = 0.21 \times 10^{-3}\,\mathrm{GPa}^{-1}$ (1.57×10^{-3}–$1.36 \times 10^{-3}\,\mathrm{GPa}^{-1}$), $\Delta\beta_2 = 0.22 \times 10^{-3}\,\mathrm{GPa}^{-1}$($1.82 \times 10^{-3}$–$1.60 \times 10^{-3}\,\mathrm{GPa}^{-1}$), $\alpha_{01} = 152.66°$ and $\alpha_{02} = 151.82°$ were used to calculate $\alpha_i(P)$.

5. Conclusion

The evolution of the atomic-scale structure of $YAlO_3$ clearly involves compression of both the YO12 and AlO6 sites. The compression of the YO12 site is anisotropic; the four longest Y–O distances are more compressible than the eight shorter Y–O bond lengths, and distortion within YO12 decreases with pressure. The YO12 site is less compressible than the AlO6 site, resulting in a decrease of the Al–O–Al tilting with pressure and thus $YAlO_3$ perovskite becomes less distorted with increasing pressure. The high-pressure behavior of $YAlO_3$ perovskite contrasts greatly with $CaSnO_3$, another $GdFeO_3$-type perovskite. Zhao et al. [8] found that the SnO6 site is less compressible than the CaO12 site and the Sn–O–Sn angles decreased with pressure. The distortion of $CaSnO_3$ therefore decreases with increasing pressure. The different response of these two perovskites to pressure can be ascribed to the relative compression of the AO12 and BO6 sites.

Acknowledgments

The authors acknowledge with gratitude the financial support for this work derived from NSF grant EAR-0105864. Ruby pressure measurements were conducted with the Raman system in the Vibrational Spectroscopy Laboratory in the Department of Geological Sciences at Virginia Tech. We thank Mr. Charles Farley for his preparing Raman facility for our ruby pressure calibration.

References

[1] A.M. Glazer, Acta Crystallogr. B 28 (1972) 3384.
[2] P.M. Woodward, Acta Crystallogr. B 52 (1997) 32.
[3] P.M. Woodward, Acta. Crystallogr. B 53 (1997) 44.
[4] A. Navrotsky, D. Weidner, in: Geophysical Monograph, Vol. 45, American Geophysical Union, Washington, DC, 1989.
[5] N.L. Ross, Phase Trans. 58 (1996) 27.
[6] N.L. Ross, Phys. Chem. Miner. 25 (1998) 597.
[7] N. Ross, R. Hazen, Phys. Chem. Miner. 17 (1990) 228.
[8] J. Zhao, N.L. Ross, R.J. Angel, Phys. Chem. Miner. (2004) accepted.
[9] D.R. Allan, R. Miletich, R.J. Angel, Rev. Sci. Instrum. 67 (1996) 840.
[10] R.J. Angel, R.T. Downs, L.W. Finger, in: R.M. Hazen, R.T. Downs (Eds.), High-Pressure, High Temperature Crystal Chemistry, Reviews in Mineralogy and Geochemistry, Vol. 41, Mineralogical of Society America, Washington, DC, 1999, pp. 559–596.
[11] H.E. King, L.W. Finger, J. Appl. Crystallogr. 12 (1979) 374.
[12] R.L. Ralph, L.W. Finger, J. Appl. Crystallogr. 15 (1982) 537.
[13] R.J. Angel, D.R. Allan, R. Miletich, L.W. Finger, J. Appl. Crystallogr. 30 (1997) 461.
[14] R.J. Angel, in: R.M. Hazen, R.T. Downs (Eds.), High-Pressure, High Temperature Crystal Chemistry, Reviews in Mineralogy and Geochemistry, Vol. 41, Mineralogical of Society America, Washington, DC, 2000, pp. 559–596.
[15] J. Orear, Am. J. Phys. 50 (1982) 912.
[16] R. Miletich, D.R. Allan, W.R. Kuhs, in: R.M. Hazen, R.T. Downs (Eds.), High-pressure, high temperature crystal chemistry, Reviews in Mineralogy and Geochemistry, Vol. 41, Mineralogical of Society America, Washington, DC, 2000, pp. 445–520.
[17] H.K. Mao, J. Xu, P.M. Bell, J. Geophys. Res. 91 (1986) 4673.
[18] H.E. King, L.W. Finger, Am. Mineral. 63 (1978) 337–342.
[19] R.J. Angel, J. Appl. Crystallogr. 36 (2003) 295.
[20] C.W. Burnham, Am. Mineral. 51 (1966) 159.

[21] L.W. Finger, E. Price, A system of Fortran IV computer program for crystal structure computations, United State National Bureau of Standards, NBS Technical note, 854, [1] Washington, DC, 1975.
[22] N. Ross, R. Angel, Am. Mineral. 84 (1999) 277.
[23] J. Kung, R.J. Angel, N.L. Ross, Phys. Chem. Miner. 28 (2001) 35.
[24] N.L. Ross, T.D. Chaplin, J. Solid State Chem. 172 (2003) 123.
[25] K. Robinson, G.V. Gibbs, P.H. Ribbe, Science 172 (1971) 567.
[26] S. Sasaki, C. Prewitt, R.C. Leibermann, Am. Mineral. 68 (1983) 1189.
[27] M. O'Keeffe, B. Hyde, J. Bovin, Phys. Chem. Miner. 4 (1979) 299.
[28] Y. Zhao, D. Weidner, J. Parise, D. Cox, Phys. Earth Planet Int. 76 (1993) 1.
[29] Y. Zhao, D. Weidner, J. Parise, D. Cox, Phys. Earth Planet Inter. 76 (1993) 17.